Automatic Control of Aircraft Lateral-directional Motion during Landing using Neural Networks and Radio-technical Subsystems

Mihai Lungu[1], Romulus Lungu[2]

[1]University of Craiova, Faculty of Electrical Engineering, 107 Decebal Blvd., Craiova, Romania, Lma1312@yahoo.com
[2]University of Craiova, Faculty of Electrical Engineering, 107 Decebal Blvd., Craiova, Romania, romulus_lungu@yahoo.com

The paper presents a new automatic architecture for the control of aircraft lateral-directional motion during landing; the system controls the lateral angular deviation of aircraft longitudinal axis with respect to the runway, by using a classical controller, a radio-navigation system, a system for the calculation of the distances between aircraft and the runway radio-markers, and an adaptive controller mainly used for the control of aircraft roll angle and its deviation with respect to the runway. The adaptive control system uses the dynamic inversion concept, a dynamic compensator, a neural network trained by the system's estimated error vector (signal provided by a linear observer), and a Pseudo Control Hedging block. The new designed adaptive architecture is software implemented and validated by complex numerical simulations; the obtained characteristics are very good and prove the new architecture's stability and its small overshoots.

Key words: Adaptive control, Dynamic inversion, Neural Network

1. Introduction

Nowadays many aircraft are equipped with automatic landing systems (ALSs) consisting of glide slope and direction radio-technical systems; for the control of the lateral motion during landing, one uses an Instrumental Landing System (ILS) type radio-navigation system together with a system for the calculation of the distances between the aircraft and the runway radio-markers [1, 2]; the direction controllers which are used within such ALSs are proportional-derivative (P.D.) type, proportional-integral (P.I.) type, proportional-integral-derivative (P.I.D.) type, in classical of fuzzy variants [1-6]. Other structures of ALSs use optimal controllers, with or without state observers [7, 8].

Because the atmospheric conditions and the dynamics of aircraft are drastically changing during flight and, of course, during landing, it is difficult to land safely by using conventional controllers. To design perfect conventional controllers, one has to know the precise mathematical model of the system to be controlled. Furthermore, the aircraft dynamics may vary with respect to altitude and flight conditions. Therefore, the adaptive controllers are better choices.

The unknown or partially known nonlinearities associated to aircraft or compensators' dynamics require the usage of different adaptive control architectures such as the ones based on the dynamic inversion technique and neural networks, with or without Pseudo Control Hedging (PCH) blocks [9-16]. The adapting and the train of the neural networks (NNs) are based on the signals provided by the observers which receive information relative to the error of the automatic control system. For a safety landing, the required information in lateral-directional plane is obtained by means of gyro transducers, accelerometers [16], or radio-technical transducers [1] whether or not the landing control architecture includes an observer.

Feedback linearization, in its various forms, is perhaps the most commonly employed nonlinear control method; it is used in [17] for nonlinear control in the design of an automatic landing system; unfortunately, the paper presents limited insight into the performance of simulations of this controller and no tests are performed outside of these simulations. To use the feedback linearization, all parametric plant uncertainties must appear in the same equation of the state-space representation as the control (the main disadvantage of the feedback linearization method).

Feed-forward neural networks based on the back propagation learning algorithm have been used in [18]; the main disadvantage is that the neural networks require a priori training on normal and faulty operating data. Other approaches involves the usage of the time delay neural networks; a controller based on this type of neural networks has been designed in [19], but its main drawback is related to the flight path track accuracy and to the fact that it is enable only under limited conditions. Several neural network control approaches have been proposed based on Lyapunov stability theory [19, 20]. The main advantage of these control schemes is that the adaptive laws were obtained from the Lyapunov synthesis and, therefore, guarantees the system's stability; the disadvantage is that some conditions should be assumed; these requirements are not easy to satisfy in practical control application [21]. Juang designed a new learning technique using a time delay network or networks with back-propagation through time algorithms to control the landing [22]; the main drawbacks are: 1) the number of hidden units was determined by trial; 2) the convergence time is high. In [23, 24] seven different neural network structures (including critic or Radial Basis Function Neural Networks) have been used for obtaining intelligent auto-landing controllers by means of linearized inverse dynamic model; also, the fuzzy logic technique was used to design controllers that track a pre-determined flight path trajectory for safe landing [25]. In the research area of optimal synthesis, Shue and Agarwal [26] have developed a mixed technique for the H_2/H_∞ control of landing, while Ochi and Kanai [27] have used the H_∞ control technique to design an approach for aircraft

automatic and landing. In these papers, the authors did not analyze the robustness of the designed controllers in the presence of sensor errors and external disturbances [28].

The auto-landing systems designed in the above mentioned works are characterized by insufficient generality or accuracy. Therefore, our aim is to develop a control system that can handle different climatic conditions and, therefore, the neural network and dynamic inversion based control system could be a solution. Thus, the paper presents a new adaptive landing architecture for aircraft control in lateral-directional plane; this study was motivated by the fact that, according to the authors of the present paper, little progress has been reported in the design of the landing flight control systems (lateral-directional plane) by using neural networks, the dynamic inversion concept, linear dynamic compensators, state observers, and PCH blocks. Also, it is interesting to see if the aircraft's trajectory during landing in lateral-directional plane can be tracked with high accuracy by a neural network based controller which uses both the dynamic inversion technique and PCH blocks. Generally, the dynamic inversion relies on the philosophy of feedback linearization; the plant nonlinearities are canceled and the closed loop plant behaves like a stable linear system. The method is characterized by simplicity in the control structure, ease of implementation, global exponential stability of the tracking error etc. [17]. On the other hand, the strong point of the neural networks is their approximation ability, these being capable to approximate an unknown system dynamics through learning. A PCH block eliminates the NNs' adapting difficulties. Taking into account the advantages of these elements (NNs, dynamic inversion, PCH blocks) and the fact that, till now, no paper deals with the control of aircraft, during landing, in lateral-directional plane by means of neural networks, dynamic inversion concept, linear dynamic compensators, state observers and PCH blocks, the present paper represent an absolute novelty in the search area of ALSs' design.

The structure of the paper is the following one: the geometry of aircraft motion in lateral-directional plane during landing and the structure of the new ALS are given in the paper's second section; the design of the new ALS's adaptive subsystems are presented in the third section; in the next section, complex simulations to validate the new designed ALS have been performed and the obtained results are analyzed; finally, some conclusions are shared in the fifth section of the paper.

2. The Geometry of Lateral-directional Motion and the Structure of the New Automatic Landing System

2.1. The geometry of the motion in lateral-directional plane

During the cruise flight, aircraft must respect the information provided by the direction marker (VOR equipment) which is used together with the equipment for the measurement of the distance R with respect to the main marker (DME equipment). During the initial approach (first landing phase), instead of the VOR marker, there is used an ILS one (together with a DME equipment) providing the direction of the runway [1].

In fig. 1 [7] one presents the geometry of aircraft motion in lateral-directional plane; ψ express the flight direction of the aircraft (the direction of the vector $\vec{V}_0$) with respect to the geographic North, V_0 – the nominal flight speed, $\overline{\psi}$ – the direction of the marker (runway), $\Delta\psi \equiv \Delta\psi_{runway} = \overline{\psi} - \psi$, λ – the deviation of aircraft longitudinal axis with respect to the runway direction, Y – the lateral deviation of aircraft with respect to the runway, R – the distance between the aircraft and the marker, $R = R_0 - V_0 t$, $R_0 = R(0)$. According to fig. 1, one writes:

$$\sin\lambda = \frac{Y}{R}, \lambda \cong 57.3\frac{Y}{R}[\text{deg}]. \tag{1}$$

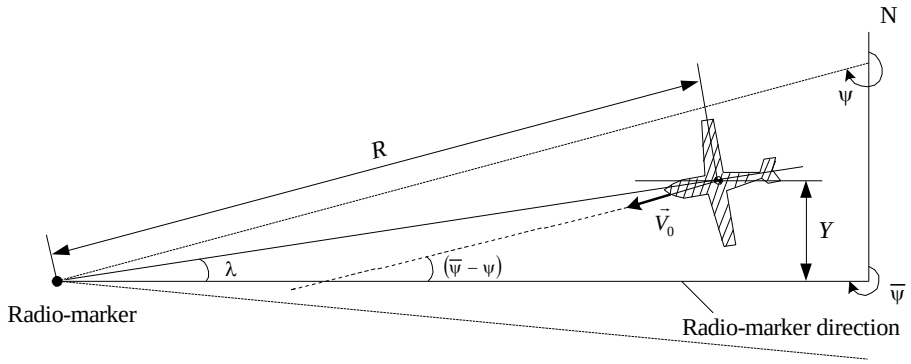

Fig. 1 The geometry of aircraft motion in latreal-directional plane

From the triangle of velocities, it follows:

$$\dot{Y} = V_0 \sin\Delta\psi = \frac{V_0}{57.3}\Delta\psi, [\Delta\psi] = \text{deg}. \tag{2}$$

If the aircraft motion is horizontal and coordinated ($\dot{\beta} = 0$, β – the aircraft sideslip angle), one obtains [3]:

$$\dot{\psi} \cong \frac{g}{V_0}\varphi_c\,, \tag{3}$$

with φ – the aircraft roll angle (lateral tilt) and g – the gravitational acceleration; this equation expresses the fact that the calculated (desired) value of the roll angle (φ_c) must be proportional to the yaw angular rate $(\varphi_c \approx \dot{\psi})$. Moreover, in order to obtain the convergence $\psi \to \psi_c$, the following condition must be fulfilled:

$$\varphi_c = k_\psi(\Delta\psi - \Delta\psi_c) = k_\psi(\psi_c - \psi) \approx \dot{Y}. \tag{4}$$

From equations (3) and (4), one gets:

$$\dot{\psi} + k_\psi \frac{g}{V_0}\psi = k_\psi \frac{g}{V_0}\psi_c\,; \tag{5}$$

thus, ψ non-periodically tends to ψ_c.

2.2. The structure of the new automatic landing system

The model of the subsystem ILS+DME is obtained below; by time derivation of equation (1) and taking into account that the term $\dot{R}Y / R^2$ can be neglected, it results:

$$\dot{\lambda} \cong 57.3\frac{\dot{Y}}{R} \overset{(2)}{=} \frac{V_0}{R}\Delta\psi \overset{(4)}{\approx} \varphi \overset{(3)}{=} \frac{V_0}{g}\dot{\psi}. \tag{6}$$

From this, it yields: $\dot{\psi} \approx \dot{Y} \approx \dot{\lambda}$ and, as a consequence,

$$\Delta\psi \to \Delta\psi_c \approx \Delta Y \approx \Delta\lambda. \tag{7}$$

In order to obtain in steady regime $\Delta\lambda = \lambda_c - \lambda = -\lambda \overset{(1)}{=} Y = 0$, a P.I. direction controller can be used and, furthermore, in order to obtain in steady regime $\Delta\dot{\lambda} = \dot{\lambda} = 0$, we introduce an additional derivative component in the controller's structure; thus, the controller becomes a P.I.D. one (fig. 2 – the structure of the automatic system for the control of aircraft lateral motion), with the transfer function [25]:

$$\frac{\Delta\psi_c(s)}{\Delta\lambda(s)} = k_c\left(1 + \frac{1}{\tau_i s} + \tau_d s\right). \tag{8}$$

From (3), one obtains:

$$\Delta\psi = \frac{g}{V_0}\frac{1}{s}\varphi. \tag{9}$$

thus, according to fig. 2, on the loop's direct way for the control of the angle $\Delta\psi$ there is an ideal integrator (after aircraft roll angle) and, therefore, in steady regime, it yields:

$$\Delta\psi_c = \Delta\psi \overset{(2)}{=} \dot{Y} \overset{(6)}{=} \dot{\psi} \equiv \omega_z \overset{(6)}{=} \dot{\lambda} \overset{(6)}{=} 0\,; \tag{10}$$

ω_z is the yaw angular rate of the aircraft.

According to equation (4) and fig. 2 (the reference models are omitted for the moment), it results: $\overline{\varphi} \equiv \varphi_c = 0$. Imposing that the adaptive control system in fig. 2 has, on its loop's direct way (for the control of the angle φ) at least an ideal integrator, then, in steady regime, one obtains: $\varphi = \varphi_c \equiv \overline{\varphi} = 0$. Also, imposing to the same loop to have on its direct way a P.D. dynamic compensator, in steady regime, the calculated roll angular rate (ω_{x_c}) and the real one (ω_x) verify the equations:

$$\omega_{x_c} \approx (\varphi_c - \varphi) = \omega_x \equiv \dot{\varphi} = 0. \tag{11}$$

Putting together all these remarks, it results that the system in fig. 2 ensures in steady regime the followings:

$$\Delta\lambda = \lambda_c = Y = \dot{Y} = \Delta\psi_c = \Delta\psi = \dot{\psi} \equiv \omega_z = \dot{\lambda} = \varphi = \varphi_c \equiv \overline{\varphi} = \dot{\varphi} \equiv \omega_x = 0. \tag{12}$$

One of the reference models' output is the vector $\bar{y} = \left[\overline{\varphi} \quad \Delta\overline{\psi}\right]^T \to y_c = \left[y_{1_c} \quad y_{2_c}\right]^T = \left[\varphi_c \quad \Delta\psi_{runway}\right]^T = \left[\varphi_c \quad 0\right]^T$.

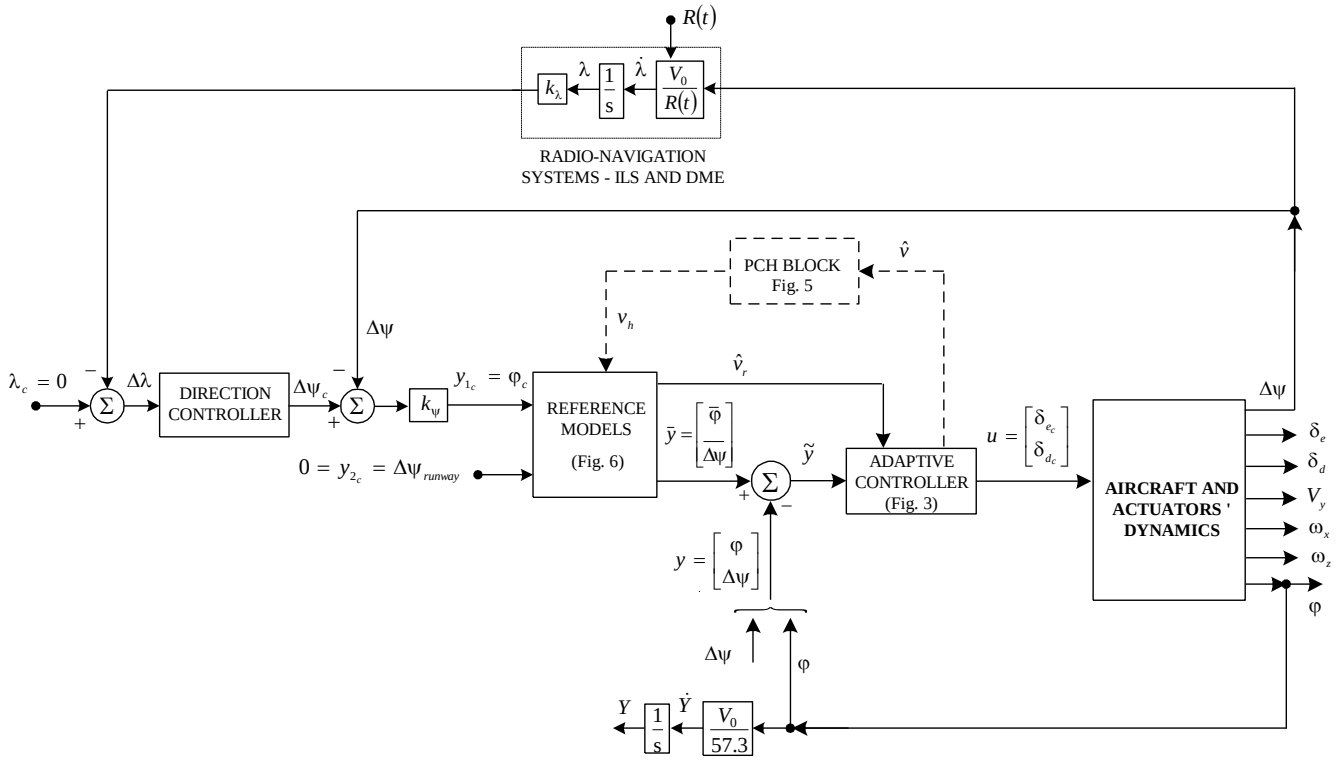

Fig. 2 Block diagram of the automatic system for the control of aircraft latreal-directional motion

3. Design of the Adaptive System for the Control of Aircraft Lateral-directional Motion

Aircraft landing is simplified if the aircraft motion in lateral-directional plane is made without errors (deviation of the aircraft from the runway direction is zero). This is why, the system for the automatic control of the flight direction is very important. Before the start of the two landing main stages in longitudinal plane (the glide slope phase and the flare phase), the pilot must cancel the aircraft lateral deviation with respect to the runway (Y) and the aircraft lateral velocity (V_y). These are the main purposes of the adaptive system to be designed in this section.

The simplified block diagram of the adaptive system for the control of aircraft lateral-directional motion from fig. 2 has an inner loop for the control of the output vector *y* (fig. 3); on its direct way, the system in fig. 3 has an adaptive controller. The control law (the pseudo-control) $\hat{v}$ has four components: 1) v_{pd} – the output of a linear dynamic compensator (for the stabilization of aircraft linear dynamics); 2) $\hat{v}_r$ – the component provided by the reference models for the cancelation of the system's deviation $\tilde{y}$ and of its derivatives; 3) v_a – the adaptive component (the output of a neural network – NN_c having the input $\eta = [\hat{v} \quad y]^T$) for the compensation of the of the approximation error ε associated to the nonlinear function $h_r(v, y)$ which interferes in the dynamics of the aircraft and of the actuators; 4) $\bar{v}$ – a robustness component.

The complete block diagram of the lateral-directional automatic control system is presented in fig. 4.

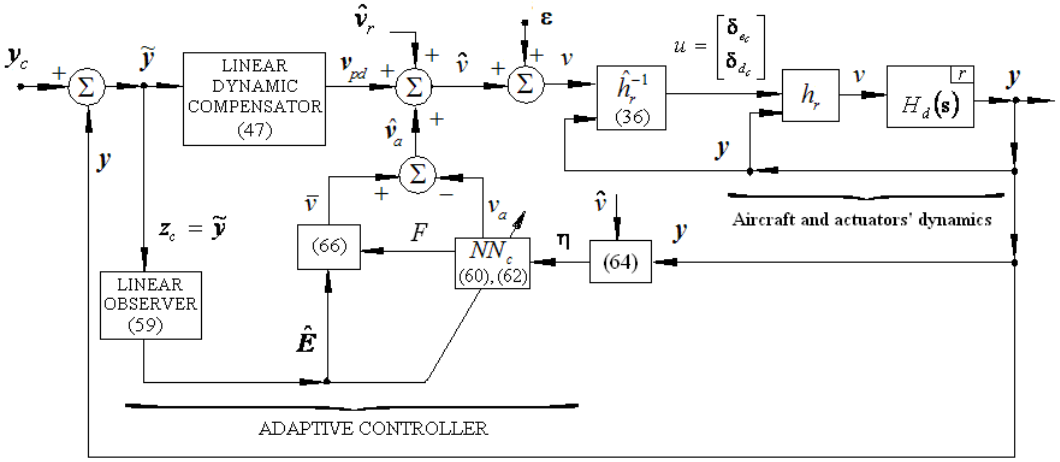

Fig. 3 The adaptive control system for the vector $y = [y \quad \Delta\psi]^T$

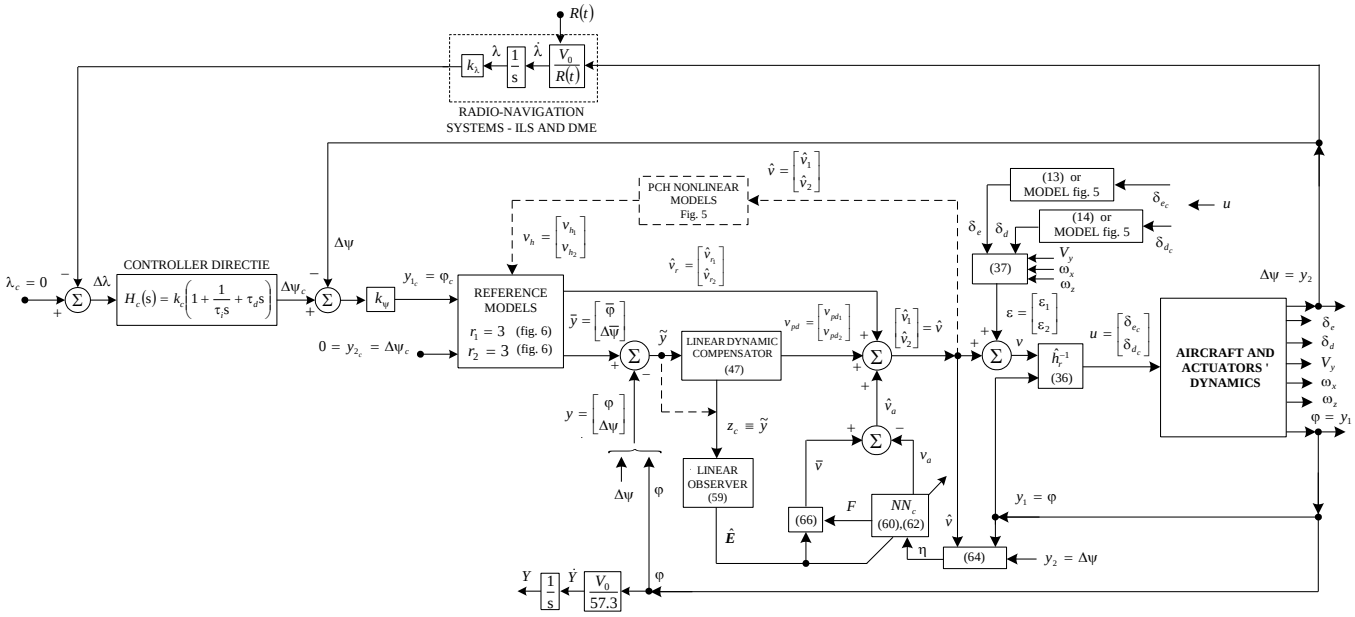

Fig. 4 Automatic landing system in lateral-directional plane

The state associated to the lateral dynamics is $\boldsymbol{x} = \begin{bmatrix} V_y & \omega_x & \omega_z & \varphi & \Delta\psi \end{bmatrix}^T$ with V_y – the lateral velocity, ω_x and ω_z – the roll and the yaw angular rates, φ – the roll angle, $\Delta\psi$ – the variation of the flight direction angle; δ_e and δ_d are the states of the actuators (δ_e – the ailerons' defection and δ_d – the rudder deflection). The actuators (the servo-aileron and the servo-rudder) are described by the linear equations:

$$T_e\dot{\delta}_e + \delta_e = \delta_{e_c}\,, \tag{13}$$

$$T_d\dot{\delta}_d + \delta_d = \delta_{d_c}\,, \tag{14}$$

or by the equations describing the nonlinear subsystems of the PCH models in fig. 5 [9], where $\overline{\delta}_i$ are replaced by δ_i ; for $i = e, \delta_{i_c} = \delta_{e_c}$ is the command of the aileron's actuator, while, for $i = d, \delta_{i_c} = \delta_{d_c}$ is the command of the actuator associated to the rudder. The command vector of the system consisting of the lateral-directional dynamics and the actuators' dynamics (linear or nonlinear) is $u = \begin{bmatrix} \delta_{e_c} & \delta_{d_c} \end{bmatrix}^T$.

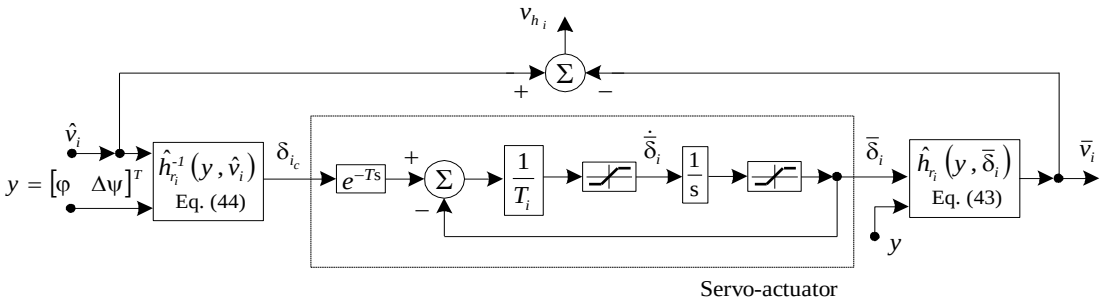

Fig. 5 Block diagram of the actuators and PCH

In linearized description, with respect to the runway direction, the aircraft dynamics in lateral-directional plane is represented by the following state equation [3]:

$$\dot{\boldsymbol{x}} = A_v\boldsymbol{x} + B_v u\,,\; A_v = \begin{bmatrix} a_{11} & 0 & a_{13} & a_{14} & 0 \\ a_{21} & a_{22} & a_{23} & 0 & 0 \\ a_{31} & a_{32} & a_{33} & 0 & 0 \\ 0 & 1 & 0 & 0 & 0 \\ 0 & 0 & 1 & 0 & 0 \end{bmatrix},\; B_v = \begin{bmatrix} 0 & b_{12} \\ b_{21} & b_{22} \\ b_{31} & b_{32} \\ 0 & 0 \\ 0 & 0 \end{bmatrix}. \tag{15}$$

The aircraft linear dynamics in lateral-directional plane is obtained (deduced) in [3] from the aircraft nonlinear dynamics $m\left(\dot{V}_y + \omega_z V_x - \omega_x V_z\right) = F_y$, $J_{xx}\dot{\omega}_x - J_{xz}\dot{\omega}_z = M_x$, $J_{zz}\dot{\omega}_z - J_{xz}\dot{\omega}_x = M_z$, by linearization and by using the exact total differential method. Here V_x and V_z are the aircraft longitudinal and vertical velocities, F_y is the resultant lateral force (*oy* – the lateral axis of the aircraft oriented towards the right wing), M_x, M_z – the resultant rotation moments of the aircraft around its longitudinal (*ox*) and vertical (*oz*) axes; J_{xx}, J_{zz} – axial inertial moments, J_{xz} – planar inertia moment. The linearization has been made around a specific operating point (regime) – flight at constant altitude, the initial angular rates (roll, pitch, and yaw angular rates) being null: $\omega_{x0} = \omega_{y0} = \omega_{z0} = 0$; the components of the weight force have been also taken into account.

The system having the input $\bar{y}$ and the output y (the inner loop of the system in fig. 2) has on its direct way the adaptive controller, the actuators and the aircraft lateral-directional dynamics. This dynamics, together with the one associated to the actuators, may be described by the state equations:

$$\dot{\boldsymbol{x}} = f(\boldsymbol{x}, u), y = h(\boldsymbol{x}), \tag{16}$$

with the state $\boldsymbol{x} = \begin{bmatrix} V_y & \omega_x & \omega_z & \varphi & \Delta\psi & \delta_e & \delta_d \end{bmatrix}^T$ and the command vector $u = \begin{bmatrix} \delta_{e_c} & \delta_{d_c} \end{bmatrix}^T$; f and h are nonlinear functions, generally unknown or linear functions obtained in the linearization process with respect to the runway's direction; in this paper, we assume that $h(\boldsymbol{x})$ is a uniquely invertible function.

Let's denote with r_i – the relative degrees of the system (16) with respect to the variables $y_i, i = \overline{1,2}$; $y_1 = \varphi, y_2 = \Delta\psi$, $y = \begin{bmatrix} y_1 & y_2 \end{bmatrix}^T$. The dynamics (16) is equivalent with the system described by the equations:

$$y_i^{(r_i)} = -\lambda_i^T Z_i + h_{r_i}(\boldsymbol{x}, u), i = \overline{1,2}, \tag{17}$$

where one has separated the derivatives (the components of the vectors Z_i) that do not depend on *u* from the components h_{r_i} depending on *u*. The vectors λ_i and Z_i have the following forms:

$$\lambda_i = \begin{bmatrix} \lambda_{0i} & \lambda_{1i} & \dots & \lambda_{r_{i-1},i} \end{bmatrix}^T, Y_i = \begin{bmatrix} y_i & \dot{y}_i & \dots & y_i^{(r_i-1)} \end{bmatrix}^T, i = \overline{1,2}. \tag{18}$$

Putting together the two equations (17), one gets the following vectorial equation:

$$y^{(r)} = -\lambda^T Z + h_r(\boldsymbol{x}, u), \tag{19}$$

where

$$\lambda = \begin{bmatrix} \lambda_1 & \lambda_2 \end{bmatrix}^T, Z = \begin{bmatrix} Z_1 & Z_2 \end{bmatrix}^T, h_r = \begin{bmatrix} h_{r_1} & h_{r_2} \end{bmatrix}^T, r = r_1 + r_2. \tag{20}$$

This system is modeled by the subsystem "*Aircraft and actuators' dynamics*" in fig. 3 (having the input *u* and the output *y*), where $H_d(\mathrm{s}) = \begin{bmatrix} H_{d_1}(\mathrm{s}) & H_{d_2}(\mathrm{s}) \end{bmatrix}^T$, with $H_{d_i}(\mathrm{s})$ – the transfer functions of the linear subsystems with the relative degrees $r_i, i = \overline{1,2}$;

$$H_{d_i}(\mathrm{s}) = \frac{1}{\mathrm{s}^{r_i} + \lambda_{r_i-1,i}\mathrm{s}^{r_i-1} + \dots \lambda_{1i}\mathrm{s} + \lambda_{0i}}, \tag{21}$$

The pseudo-control (control law) $\hat{v}$ represents the best approximation of the vectorial function $v = h_r(\boldsymbol{x}, u) = h_r(\boldsymbol{x}(y), u) = h_r(y, u)$; let us consider that this is $\hat{v} = \hat{h}_r(y, \hat{u})$. Because

$$u = h_r^{-1}(y, v) \neq \hat{u} = \hat{h}_r^{-1}(y, \hat{v}), \tag{22}$$

it results that there is an approximation error $\varepsilon = \begin{bmatrix} \varepsilon_1 & \varepsilon_2 \end{bmatrix}^T$ which acts like a disturbance;

$$\varepsilon = h_r(y, u) - \hat{h}_r(y, \hat{u}). \tag{23}$$

If $\hat{h}_r \equiv h_r$, then

$$h_r(y, u) = h_r(y, h_r^{-1}(y, v)) = v = \hat{v} \tag{24}$$

and the equation (19) becomes:

$$y^{(r)} + \lambda^T Z = v, v = \hat{v}; \tag{25}$$

if $\hat{h}_r \neq h_r$, the equation (19) gets the form:

$$y^{(r)} + \lambda^T Z = v = \hat{v} + \varepsilon; \tag{26}$$

$$\hat{v} = \hat{v}_r + v_{pd} - v_a + \bar{v}. \tag{27}$$

For the calculation of the relative degrees r_1 and r_2, one eliminates δ_e and δ_d between the equations associated to aircraft dynamics and the actuators' dynamics, this being achieved by derivation of $\dot{\omega}_x = \ddot{\varphi}$ and $\dot{\omega}_z = \Delta\ddot{\psi}$. Then, one obtains the equations (17) with $\lambda_{01} = \lambda_{11} = 0, \lambda_{21} = 1$ and $\lambda_{02} = \lambda_{12} = 0, \lambda_{22} = 1;$ the following equations result:

$$\dddot{\varphi} + \ddot{\varphi} = c_1 V_y + c_2 \omega_x + c_3 \omega_z + c_4 \varphi + c_e \delta_e + c_d \delta_d + \frac{b_{21}}{T_e}\delta_{e_c} + \frac{b_{22}}{T_d}\delta_{d_c}, \tag{28}$$

$$\Delta\dddot{\psi} + \Delta\ddot{\psi} = d_1 V_y + d_2 \omega_x + d_3 \omega_z + d_4 \varphi + d_e \delta_e + d_d \delta_d + \frac{b_{31}}{T_e}\delta_{e_c} + \frac{b_{32}}{T_d}\delta_{d_c}, \tag{29}$$

with the notations:

$$\begin{aligned} &c_1 = a_{21}a_{11} + a_{22}a_{21} + a_{23}a_{31} + a_{21}, c_2 = a_{22}^2 + a_{23}a_{32} + a_{22}, c_3 = a_{21}a_{13} + a_{22}a_{23} + a_{23}a_{33} + a_{23}, \\ &c_4 = a_{21}a_{14}, c_e = a_{22}b_{21} + a_{23}b_{31} - b_{21}/T_e + b_{21}, c_d = a_{21}b_{12} + a_{22}b_{22} + a_{23}b_{32} - b_{22}/T_d + b_{22}, \end{aligned} \tag{30}$$

$$\begin{aligned} &d_1 = a_{31}a_{11} + a_{32}a_{21} + a_{33}a_{31} + a_{31}, d_2 = a_{32}a_{22} + a_{33}a_{32} + a_{32}, d_3 = a_{31}a_{13} + a_{32}a_{23} + a_{33}^2 + a_{33}, \\ &d_4 = a_{31}a_{14}, d_e = a_{32}b_{21} + a_{33}b_{31} - b_{31}/T_e + b_{31}, d_d = a_{31}b_{12} + a_{32}b_{22} + a_{33}b_{32} - b_{32}/T_d + b_{32}. \end{aligned} \tag{31}$$

Thus, the relative degrees are: $r_1 = r_2 = 3, r = 6.$ Therefore, the transfer functions $H_{d_i}(\mathrm{s})$ have the forms:

$$H_{d_i}(\mathrm{s}) = \frac{1}{\mathrm{s}^2(\mathrm{s}+1)}, i = \overline{1,2}. \tag{32}$$

Now, putting together the equations (28) and (29), one obtains:

$$\begin{bmatrix} \dddot{\varphi} + \ddot{\varphi} \\ \Delta\dddot{\psi} + \Delta\ddot{\psi} \end{bmatrix} = \begin{bmatrix} c_1 & c_2 & c_3 & c_4 & 0 & c_e & c_d \\ d_1 & d_2 & d_3 & d_4 & 0 & d_e & d_d \end{bmatrix} \boldsymbol{x} + \begin{bmatrix} \frac{b_{21}}{T_e} & \frac{b_{22}}{T_d} \\ \frac{b_{31}}{T_e} & \frac{b_{32}}{T_d} \end{bmatrix} \begin{bmatrix} \delta_{e_c} \\ \delta_{d_c} \end{bmatrix}, \tag{33}$$

which has the form:

$$y^{(r)} = h_r(y,u), h_r(y,u) = h_r\left(y, \hat{h}_r^{-1}(y,v)\right) \cong v = \hat{v} + \varepsilon. \tag{34}$$

This equation has also the form (26); by identification of the right side of equations (33) and (34), it yields:

$$\hat{v} = \begin{bmatrix} \hat{v}_1 \\ \hat{v}_2 \end{bmatrix} = \begin{bmatrix} \hat{h}_{r_1}(y,\hat{u}) \\ \hat{h}_{r_2}(y,\hat{u}) \end{bmatrix} = \begin{bmatrix} \hat{h}_{r_1}(\varphi, \Delta\psi, \delta_{e_c}, \delta_{d_c}) \\ \hat{h}_{r_2}(\varphi, \Delta\psi, \delta_{e_c}, \delta_{d_c}) \end{bmatrix} = \begin{bmatrix} c_4 \\ d_4 \end{bmatrix} \varphi + \begin{bmatrix} \frac{b_{21}}{T_e} & \frac{b_{22}}{T_d} \\ \frac{b_{31}}{T_e} & \frac{b_{32}}{T_d} \end{bmatrix} \begin{bmatrix} \hat{\delta}_{e_c} \\ \hat{\delta}_{d_c} \end{bmatrix} \tag{35}$$

or

$$\hat{u} = \begin{bmatrix} \hat{\delta}_{e_c} \\ \hat{\delta}_{d_c} \end{bmatrix} = \hat{h}_r^{-1}(y,\hat{v}) = \begin{bmatrix} \frac{b_{21}}{T_e} & \frac{b_{22}}{T_d} \\ \frac{b_{31}}{T_e} & \frac{b_{32}}{T_d} \end{bmatrix}^{-1} \left\{ \hat{v} - \begin{bmatrix} c_4 \\ d_4 \end{bmatrix} \varphi \right\} \tag{36}$$

and

$$\varepsilon = \begin{bmatrix} \varepsilon_1 \\ \varepsilon_2 \end{bmatrix} = \begin{bmatrix} c_1 & c_2 & c_3 & c_e & c_d \\ d_1 & d_2 & d_3 & d_e & d_d \end{bmatrix} \begin{bmatrix} V_y & \omega_x & \omega_z & \delta_e & \delta_d \end{bmatrix}^T. \tag{37}$$

In order to obtain the control law u with respect to $\hat{u}$ and ε, one uses the Taylor series expansion of the function $u = h_r^{-1}(y,v)$ around the pair of variables $(y, \bar{v})$ and gets:

$$u = h_r^{-1}(y, v) \cong \hat{h}_r^{-1}(y, \hat{v}) + \frac{\mathrm{d}}{\mathrm{d}v}\left(h_r^{-1}(y, v)\right)_{v=\bar{v}}(v - \hat{v}) = \hat{u} + \frac{\mathrm{d}}{\mathrm{d}\hat{v}}\left(\hat{h}_r^{-1}(y, \hat{v})\right)\varepsilon. \tag{38}$$

Replacing the expression of $\hat{h}_r^{-1}(y, \hat{v})$ (form (36)) into (38), one obtains:

$$u = \begin{bmatrix} \delta_{e_c} \\ \delta_{d_c} \end{bmatrix} = \begin{bmatrix} \frac{b_{21}}{T_e} & \frac{b_{22}}{T_d} \\ \frac{b_{31}}{T_e} & \frac{b_{32}}{T_d} \end{bmatrix}^{-1} \left\{ v - \begin{bmatrix} c_4 \\ d_4 \end{bmatrix} \varphi \right\}. \tag{39}$$

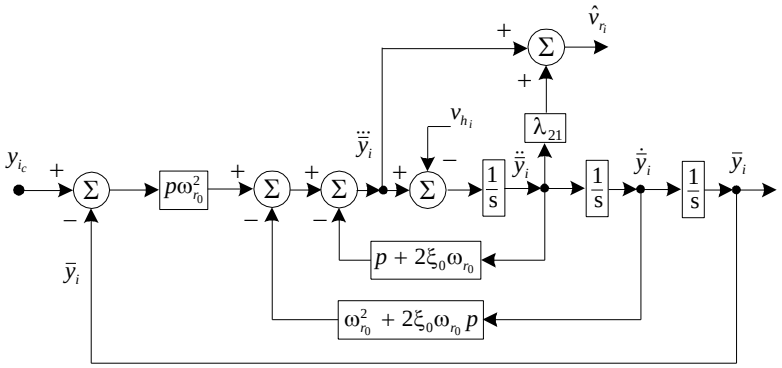

Fig. 6 Block diagram of the reference models

Taking into account that the transfer functions of the reduced order linear subsystems have the forms (32), one can choose identical three order reference models with the transfer functions:

$$\frac{\bar{y}_i(\mathrm{s})}{y_{i_c}(\mathrm{s})} = \frac{p\omega_{r_0}^2}{(\mathrm{s} + p)\left(\mathrm{s}^2 + 2\xi_0\omega_{r_0}\mathrm{s} + \omega_{r_0}^2\right)}, i = \overline{1,2}, \tag{40}$$

modeled by the block diagram in fig. 6; beside $\bar{y}_i$, from the block diagram in fig. 6, one also gets the components $\hat{v}_{r_i}$ of the vector $\hat{v}_r = \begin{bmatrix} \hat{v}_{r_1} & \hat{v}_{r_2} \end{bmatrix}^T$, obtained from the condition that *y* and its derivatives are equal to the imposed ones, i.e. $y^{(r)} = \bar{y}^{(r)}$ and $Z = \bar{Z}$, this being achieved in steady regime when $v_a = \varepsilon$ (the approximation error is compensated by the adaptive components v_a); thus, in (26), $\varepsilon = 0$ and, from this equation, it results:

$$\hat{v}_r = \bar{y}^{(r)} + \lambda^T \bar{Z}, \tag{41}$$

with $\lambda = \begin{bmatrix} \lambda_1 & \lambda_2 \end{bmatrix}^T \overset{(18)}{=} \begin{bmatrix} 0 & 0 & 1 & 0 & 0 & 1 \end{bmatrix}^T$. Thus, $\hat{v}_{r_i} = \dddot{\bar{y}}_i + \ddot{\bar{y}}_i$.

The signals v_{h_i} from the block diagram in fig. 6 are the components of the vector v_h – the output of the PCH nonlinear model (see figs. 2 and 4), consisting of two subsystems having the architectures in fig. 5 [9]. The PCH block is introduced when the actuators (the servo-aileron and the servo-rudder) are nonlinear, issue which affects the neural networks; the neural networks are sensitive to actuator nonlinearities, while the PCH blocks eliminate the NNS' adapting difficulties. Generally, PCH "moves back" the reference model, introducing correction responses of the reference models with respect to the estimation of the execution element's position. The signals provided by PCH (v_{h_i}) are additional inputs of the reference models, forcing these to "go back" [9].

In order to obtain the components $\hat{h}_{r_i}$ and $\hat{h}_{r_i}^{-1}$, one expresses the components $\hat{v}_i, i = \overline{1,2}$ from (35); in the equation of $\hat{v}_1$, the term containing $\hat{\delta}_{d_c}$ is omitted, while, in the equation of $\hat{v}_2$, the term containing $\hat{\delta}_{e_c}$ is neglected due to the independence between the roll and the yaw channels; it yields:

$$\hat{v}_1 = c_4\varphi + \frac{b_{21}}{T_e}\hat{\delta}_{e_c}, \hat{v}_2 = d_4\varphi + \frac{b_{32}}{T_d}\hat{\delta}_{d_c}. \tag{42}$$

Taking into account the notations in fig. 5 ($\hat{v}_i$ becomes $\bar{v}_i$ and $\hat{\delta}_{i_c}$ becomes $\bar{\delta}_i$ for the blocks $\hat{h}_{r_i}(y, \bar{\delta}_i)$ and δ_{i_c} for the blocks $\hat{h}_{r_i}^{-1}(y, \hat{v}_i)$, respectively), the following functions result:

$$\bar{v}_1 = \hat{h}_{r_1}\left(y, \bar{\delta}_1\right) = \hat{h}_{r_1}\left(y, \bar{\delta}_e\right) = c_4\varphi + \frac{b_{21}}{T_e}\bar{\delta}_e, \bar{v}_2 = \hat{h}_{r_2}\left(y, \bar{\delta}_2\right) = \hat{h}_{r_2}\left(y, \bar{\delta}_d\right) = d_4\varphi + \frac{b_{32}}{T_d}\bar{\delta}_d; \tag{43}$$

$$\delta_{e_c} = \hat{h}_{r_1}^{-1}\left(y, \hat{v}_1\right) = \hat{h}_{r_1}^{-1}\left(\varphi, \hat{v}_1\right) = \frac{T_e}{b_{21}}\left(\hat{v}_1 - c_4\varphi\right), \delta_{d_c} = \hat{h}_{r_2}^{-1}\left(y, \hat{v}_2\right) = \hat{h}_{r_2}^{-1}\left(\varphi, \hat{v}_2\right) = \frac{T_d}{b_{32}}\left(\hat{v}_2 - d_4\varphi\right). \tag{44}$$

The system in fig. 3 has the state vector $\boldsymbol{E} = \left[\tilde{y} \;\; \dot{\tilde{y}} \;\; \ddot{\tilde{y}}\right]^T = \left[E \;\; \dot{E} \;\; \ddot{E}\right]^T = \left[\tilde{y}_1 \;\; \dot{\tilde{y}}_1 \;\; \ddot{\tilde{y}}_1 \;\; \tilde{y}_2 \;\; \dot{\tilde{y}}_2 \;\; \ddot{\tilde{y}}_2\right]^T$ having the order *r*=6. If we choose a P.D. linear dynamic compensator, its state is $\boldsymbol{E} = \left[E_1 \;\; E_2\right]^T = \tilde{y} = \left[\tilde{y}_1 \;\; \tilde{y}_2\right]^T = \left[\tilde{\varphi} \;\; \Delta\tilde{\psi}\right]^T$, with $\tilde{\varphi} = \bar{\varphi} - \varphi$ and $\Delta\tilde{\psi} = \Delta\bar{\psi} - \Delta\psi$. The components of the P.D. dynamic compensator's output, for the two reduced order systems, and the output vector of the P.D. dynamic compensator are respectively expressed as:

$$v_{pd_i} = k_{p_i}\tilde{y}_i + k_{d_i}\dot{\tilde{y}}_i = \left[k_{p_i} \;\; k_{d_i} \;\; 0\right]\left[\tilde{y}_i \;\; \dot{\tilde{y}}_i \;\; \ddot{\tilde{y}}_i\right]^T = d_{c_i}\boldsymbol{E}_i, \tag{45}$$

where

$$d_{c_i} = \left[k_{p_i} \;\; k_{d_i} \;\; 0\right], \boldsymbol{E}_i = \left[\tilde{y}_i \;\; \dot{\tilde{y}}_i \;\; \ddot{\tilde{y}}_i\right]^T, i = \overline{1,2}; \tag{46}$$

$$v_{pd} = \left[v_{pd_1} \;\; v_{pd_2}\right]^T = \left[d_{c_1}\boldsymbol{E}_1 \;\; d_{c_2}\boldsymbol{E}_2\right]^T = D_c\left[\boldsymbol{E}_1 \;\; \boldsymbol{E}_2\right]^T = D_c\boldsymbol{E}, \tag{47}$$

with

$$D_c = \begin{bmatrix} d_{c_1} & 0_{1\times 3} \\ 0_{1\times 3} & d_{c_2} \end{bmatrix} = \begin{bmatrix} k_{p_1} & k_{d_1} & 0 & 0 & 0 & 0 \\ 0 & 0 & 0 & k_{p_2} & k_{d_2} & 0 \end{bmatrix}. \tag{48}$$

Taking into consideration that the transfer functions of the two reduced order systems (having the outputs $y_i, y_1 = \varphi$, $y_2 = \Delta\psi$) have the forms (32), it results that these subsystems may be described by the state equations:

$$\dot{Z}_i = A_i Z_i + B_i v_i, i = \overline{1,2}, v_i = v_{pd_i} + \hat{v}_{r_i} + \hat{v}_{a_i} + \varepsilon_i, \tag{49}$$

with

$$A_1 = A_2 = \begin{bmatrix} 0 & 1 & 0 \\ 0 & 0 & 1 \\ 0 & 0 & -1 \end{bmatrix}, B_1 = \begin{bmatrix} 0 & 0 \\ 0 & 0 \\ 1 & 0 \end{bmatrix}, B_2 = \begin{bmatrix} 0 & 0 \\ 0 & 0 \\ 0 & 1 \end{bmatrix}. \tag{50}$$

Putting together the two equations (45), one obtains the vectorial equation of the reduced order subsystem, having the input *v*, the output *y*, and the transfer matrix $H_d(\mathrm{s})$;

$$\dot{Z} = AZ + Bv, v = v_{pd} + \hat{v}_r + \hat{v}_a + \varepsilon, \tag{51}$$

with

$$A = \begin{bmatrix} A_1 & 0_{3\times 3} \\ 0_{3\times 3} & A_2 \end{bmatrix} = \begin{bmatrix} 0 & 1 & 0 & 0 & 0 & 0 \\ 0 & 0 & 1 & 0 & 0 & 0 \\ 0 & 0 & -1 & 0 & 0 & 0 \\ 0 & 0 & 0 & 0 & 1 & 0 \\ 0 & 0 & 0 & 0 & 0 & 1 \\ 0 & 0 & 0 & 0 & 0 & -1 \end{bmatrix}, B = \begin{bmatrix} B_1 & B_2 \end{bmatrix}^T = \begin{bmatrix} 0 & 0 & 1 & 0 & 0 & 0 \\ 0 & 0 & 0 & 0 & 0 & 1 \end{bmatrix}^T. \tag{52}$$

The stabilized state $\bar{Z}$ of the system (51) verifies the equation $\dot{\bar{Z}} = 0$ if and only if $A\bar{Z} = 0$ (in steady regime, one has $\hat{v} = \varepsilon = v = 0$). Subtracting from equation $A\bar{Z} = 0$ the equation (51), one obtains the state equation of the error model:

$$\dot{\boldsymbol{E}} = A\boldsymbol{E} - Bv, v = v_{pd} + \hat{v}_r + \hat{v}_a + \varepsilon, \tag{53}$$

with $\boldsymbol{E} = \bar{Z} - Z = \left[\boldsymbol{E}_1 \;\; \boldsymbol{E}_2\right]^T$. Replacing in (53) $v_{pd} = D_c\boldsymbol{E}$, this equation gets the form:

$$\dot{\boldsymbol{E}} = \bar{A}\boldsymbol{E} - \bar{B}\left(\hat{v}_r + \hat{v}_a + \varepsilon\right), \hat{v}_a = \bar{v} - v_a, \tag{54}$$

with

$$\overline{A} = A - BD_c\,,\ \overline{B} = B. \tag{55}$$

The linear observer estimates the vector $\boldsymbol{E}$ by using only the deviation of the system in fig. 3; the input of the linear observer is:

$$z_c \equiv \tilde{y} \equiv \boldsymbol{e} = \begin{bmatrix}\tilde{y}_1 & \tilde{y}_2\end{bmatrix}^T = \begin{bmatrix}c_1\boldsymbol{E}_1 & c_2\,\boldsymbol{E}_2\end{bmatrix}^T = \begin{bmatrix}c_1 & 0\\ 0 & c_2\end{bmatrix}\boldsymbol{E} = C\boldsymbol{E}\,, \tag{56}$$

with

$$C = \begin{bmatrix}c_1 & 0\\ 0 & c_2\end{bmatrix}, c_1 = c_2 = \begin{bmatrix}1 & 0 & 0\end{bmatrix}. \tag{57}$$

The equation of the observer has been borrowed from [8]:

$$\dot{\hat{\boldsymbol{E}}} = \overline{A}\hat{\boldsymbol{E}} + L\left(z_c - \hat{z}_c\right), z_c = C\boldsymbol{E}\,, \hat{z}_c = C\hat{\boldsymbol{E}}\,; \tag{58}$$

its equivalent form is:

$$\dot{\hat{\boldsymbol{E}}} = \tilde{A}\hat{\boldsymbol{E}} + L\,z_c\,, \tilde{A} = \overline{A} - L\overline{C}\,, \tag{59}$$

where L is the gain matrix of the observer; this matrix is to be obtained such that the matrix $\tilde{A}$ is asymptotically stable. As an alternative for the observer used here we can use the fuzzy state observer designed in [29].

The adaptive control law is calculated by using the formula [13]:

$$v_a = W^T\sigma\left(V^T\eta\right); \tag{60}$$

in (60) W and V are the weights of a neural network (NN_c), their dimensions being $\left(n_2+1\right)\times n_3$ and $\left(n_1+1\right)\times n_2$, respectively; the elements of W are the weights of the links between the n_2 neurons of the hidden layer and the n_3 neurons of the output layer; V has as elements the weights of the links between the n_1 neurons of the input layer and the n_2 neurons of the hidden layer. We considered that NN_c is a feed-forward type neural network having 3 layers: an input layer, a hidden layer, and an output one. In (60), the vector η is the input vector of the neural network, while $\sigma(z) = \sigma\left(V^T\eta\right)$ is a sigmoid function with the form [16]:

$$\sigma(z) = \left(1 + e^{-\alpha z}\right)^{-1}, a = \begin{bmatrix}a_1 & \dots & a_{n_1+1}\end{bmatrix}^T, \tag{61}$$

$a_j\,,\ j = \overline{1,\left(n_1+1\right)}$, being the activation potentials whose values are different for each neuron.

The matrices W and V are the solutions of the differential equations' system [9]:

$$\begin{aligned}\dot{W} &= -k_W\left[2\left(\sigma - \sigma' V^T\eta\right)\hat{\boldsymbol{E}}^{\boldsymbol{T}}P\overline{B} + k\left(W - W_0\right)\right], W_0 = W(0),\\ \dot{V} &= -k_V\left[2\eta\hat{\boldsymbol{E}}^{\boldsymbol{T}}P\overline{B}W^T\sigma' + k\left(V - V_0\right)\right], V_0 = V(0),\end{aligned} \tag{62}$$

with $\sigma' = \left.\dfrac{\mathrm{d}\sigma}{\mathrm{dz}}\right|_{z=z_0}$, k_W, k_V – positive constants, while $P\left(r\times r\right)$ is the solution of the Lyapunov equation:

$$\overline{A}^T P + P\overline{A} = -Q\,, \tag{63}$$

with $Q-$ positive defined matrix.

The input vector of the neural network (η) has the form [13]:

$$\eta = \begin{bmatrix}1 & \hat{v}_d^T & y_d^T\end{bmatrix}^T = \begin{bmatrix}1 & I_1 & I_2 & \dots & I_{n1}\end{bmatrix}^T, \tag{64}$$

$$\hat{v}_d^T = \left[\hat{v}(t)\ \ \hat{v}(t-d)\ \dots\ \hat{v}\left(t-\left(n_1-r-2\right)d\right)\right], y_d^T = \left[y(t)\ \ y(t-d)\ \dots\ y\left(t-\left(n_1-r-3\right)d\right)\right], \tag{65}$$

where $I_j\,,\ j = \overline{1,n_1}$, are the outputs of the neural network, while $d-$ the sample time.

The robustness component of the control law is calculated by means of the formula [9, 12, 13]:

$$\bar{v}^T = k_z\left(\left\|F\right\|_f + \overline{F}\right)\left\|\hat{\boldsymbol{E}}\right\|\frac{\hat{\boldsymbol{E}}^{\boldsymbol{T}}P\overline{B}}{\left\|\hat{\boldsymbol{E}}^{\boldsymbol{T}}P\overline{B}\right\|} + k_e\hat{\boldsymbol{E}}^{\boldsymbol{T}}P\overline{B}\,, \tag{66}$$

with k_z and k_e – positive gains, $F = \begin{bmatrix} W & 0 \\ 0 & V \end{bmatrix}$; $\|F\|_f^2 = \text{trace}\{F^T F\} \le \bar{F}$; $\|F\|_f$ is the Frobenius norm of the matrix *F*, while $\bar{F}$ is the ideal matrix of the neural network. The robustness component (66) ensures the boundedness of the neural network's matrices *W* and *V*. This equation has been deduced by Calise et al. and used in the adaptive control of different aerospace vehicles, using the dynamic inversion and neural networks [9, 12, 13].

Now, we make a brief stability analysis of the system in fig. 4:

1. *The stability of the inner loop* (the system having the input $\bar{y}$ and the output y): the adaptive control law v_a (form (60) with *W* and *V* described by (62)) and the robustness component $\bar{v}$ have to compensate the approximation error ε; the form of the control law resulted from the condition that the system is global asymptotically stable is $\dot{V}_a < 0$, where the chosen Lyapunov function have the form $V_a = \boldsymbol{E}^T P \boldsymbol{E} + f(W, V)$. The system having the input $(v_a - (\bar{v} + \varepsilon))$ and the state $\boldsymbol{E}$ is described by equation (54), with the function $f(W, V)$ borrowed from [11] imposing that $\dot{f}(W, V) = 0$; it resulted the equations (62) and $\dot{V}_a = -\boldsymbol{E}^T Q \boldsymbol{E} < 0$, Q having the form (63). By composing the function h_r with $\hat{h}_r^{-1}$ and by introducing the approximation error ε, the inner loop system (having the input $(v_a - (\bar{v} + \varepsilon))$ and unitary negative reaction after y) becomes linear; it has on its direct way the transfer matrix $\frac{k_p + k_d s}{s^2(s+1)}$. The determination methodology of the dynamic compensator's coefficients $k_p = \lfloor k_{p_1} \quad k_{p_2} \rfloor$ and $k_d = \lfloor k_{d_1} \quad k_{d_2} \rfloor$ is presented below and involves stability conditions for the linear system.

2. *The stability of the intermediate loop* (the linear system having the input $\Delta\psi_c$ and the output $\Delta\psi$): the system has unitary negative reaction after $\Delta\psi$ and on its direct way the series of the following systems: a proportional one (having the transmission ratio k_ψ), the reference model with the transfer function (40), and the linear inner loop system with the transfer function $H_i(s) = \frac{k_{p_2} + k_{d_2} s}{s^3 + s^2 + k_{d_2} s + k_{p_2}}$. Choosing negative roots for the characteristic equation of this system (stability condition), it results the value of the transmission ratio k_ψ.

3. *The stability of the outer loop* (the linear system having the input λ_c and the output $\Delta\psi$): following the same procedure as above, e.g. imposing negative roots for the afferent characteristic equation, one obtains the coefficients of the direction controller (k_c, τ_i and τ_d). ■

Concluding, the synthesis (the design) of the system in fig. 4 involves the calculation of the controllers' coefficients in conditions of stability.

4. Numerical Simulation Results

To study the functionality of the new designed adaptive system for the control of aircraft lateral-directional motion, we consider a light aircraft (Charlie type) having the matrices (15) of the following forms [2]:

$$A_v = \begin{bmatrix} -0.089 & 0 & -67 & 9.81 & 0 \\ -1.33 & -0.98 & 0.33 & 0 & 0 \\ 0.17 & -0.17 & -0.217 & 0 & 0 \\ 0 & 1 & 0 & 0 & 0 \\ 0 & 0 & 1 & 0 & 0 \end{bmatrix}, B_v = \begin{bmatrix} 0 & 1 \\ 0.23 & 0.06 \\ 0.026 & -0.15 \\ 0 & 0 \\ 0 & 0 \end{bmatrix}. \quad (67)$$

By using the elements of the two matrices, we calculate the coefficients (30) and (31); $T_e = T_d = 0.4\,\text{s}, T = 0.01\,\text{s}$. The coefficients of the reference models have the following values: $p = 0.5, \omega_{r_0} = 0.9\,\text{rad/s}, \xi_0 = 0.7$; the control limits of the servo-actuators are $\pm 5\,\text{deg}$ and $\pm 5\,\text{deg/s}$, respectively. The values of the dynamic compensator's parameters are calculated by using the characteristic equations of the linear subsystems (closed by unitary negative feedbacks) having the inputs $\bar{\varphi}$ and $\Delta\bar{\psi}$, the blocks $(k_{p_i} + k_{d_i} s)$ on the direct ways of these two systems in series with the blocks which have the transfer functions $H_{d_i}(s)$ (equations (32)); imposing for the characteristic equations:

$$s^3 + s^2 + k_{d_i} s + k_{p_i} = 0, i = \overline{1,2}, \quad (68)$$

negative roots (e.g. -0.1, -0.2, -0.3 and -1.1, -0.7, -0.6, respectively), it results: $k_{p_1} = 0.0193, k_{d_1} = 0.27, k_{p_2} = 0.77, k_{d_2} = 0.8$.

With these, the matrix D_c is calculated by using equation (48) and, then, by means of (52) and (55) the matrices $\overline{A}$ and $\overline{B}$ are determined. Using these matrices, choosing for the matrix $\widetilde{A} = \overline{A} - L\overline{C}$ the eigenvalues: $-1, -0.5, -0.3, -6, -7, -0.5$, the gain matrix of the observer is obtained; then, choosing the matrix $Q = 0.1 I_{6\times 6}$, the solution of the equation (63) is determined.

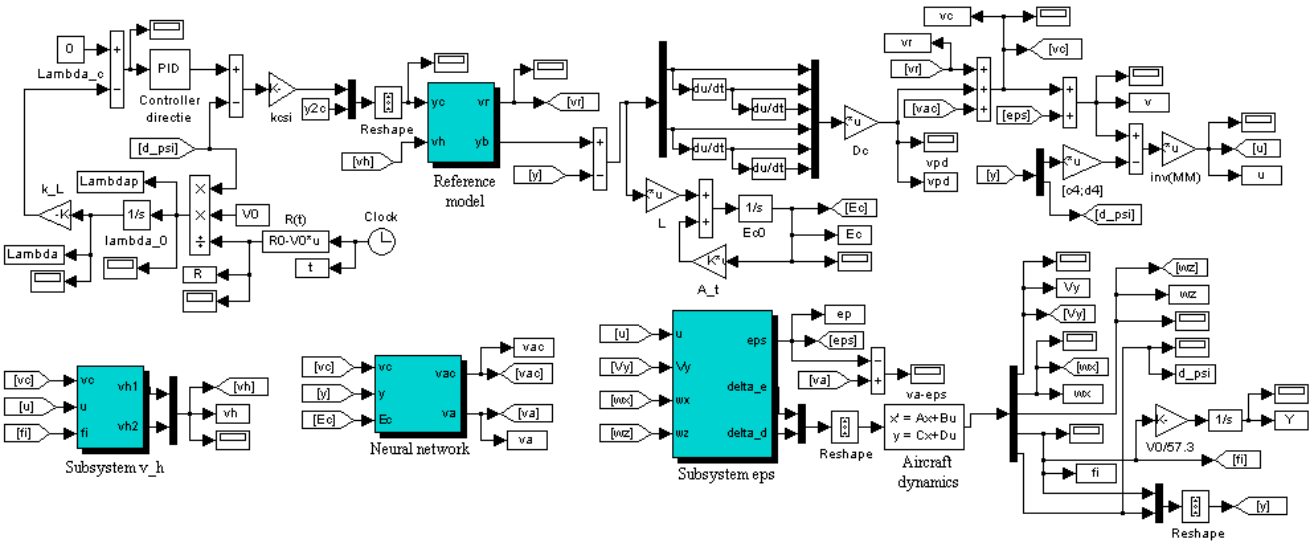

Fig. 7 Matlab/Simulink model for the new adaptive control system

With this matrix, we calculate $\hat{\boldsymbol{E}}$ – solution of equation (59) and, then, the matrices of the neural network (W and V) – solution of the system (62), with $k_W = 0.05, = k_V = 0.5, W_0 = W(0) = 0_{11\times 2}, V_0 = V(0) = 0_{10\times 10}, k = 20$. Using these, we calculate the adaptive signal v_a by means of equation (60), with η of form (64), and σ having the form (61). For the neural network (NNc) we have chosen: $n_1 = 9, n_2 = 10, n_3 = 2, d = 0.05$; the vector of activation potentials is chosen of form: $a = [1 \quad 0.9 \quad 0.8 \quad 0.7 \quad 0.6 \quad 0.5 \quad 0.4 \quad 0.3 \quad 0.2 \quad 0.1]$; $\bar{v}$ is determined by using (66), with $k_z = 0.01, k_e = 0.05, \overline{F} = 10$. To calculate the parameters of the direction controller (see fig. 4), we impose negative roots for the linear subsystem which has on feedback way the direction controller in series with the subsystem (closed by unitary negative feedbacks) having the input $\Delta\psi_c$ and the output $\Delta\psi$; in turn, this subsystem has on its direct way one of the two reference models and the adaptive control subsystem; it resulted: $\tau_i = 100\,\text{s}, \tau_d = 0.1\,\text{s}, k_\psi = 0.5$. For the navigation system, $k_\lambda = 1\,\text{V/deg}, R_0 = R(0) = 6700\,\text{m}$.

The new designed architecture in fig. 4 is software implemented in Matlab/Simulink environment – fig. 7; we obtained the time characteristics in fig. 8 (**case 1**: linear servo-actuators) and in fig. 9 (**case 2**: nonlinear servo-actuators). If the actuators are nonlinear, it is good to use a PCH block $(v_h \neq 0)$ because this allows the system to work in the linear zones of the nonlinearities. As we already stated above, the signal provided by the PCH block is a reference model's additional input. Thus, in this paper, we analyze the influence of Pseudo Control Hedging usage on the variables describing the new designed control system for aircraft motion in lateral-directional plane during landing.

From figs. 8 and 9 we remark the cancel of the following variables: the lateral velocity (V_y), the lateral deviation (Y), the roll angle and angular rate (φ, ω_x), the yaw angle and angular rate $(\Delta\psi, \omega_z)$, and the deviation of aircraft longitudinal axis with respect to the runway direction (λ); this confirms the fulfillment of the equations (10) and (12). Also, in steady regime, the command variables ($u_1 = \delta_{e_c}$ and $u_2 = \delta_{d_c}$) as well as the deflections of the ailerons and direction (δ_e and δ_d) cancel. There are also stabilized to zero: the components of the approximation vector ε (ε_1 and ε_2), the components of the pseudo-command $\hat{v}$ ($\hat{v}_1$ and $\hat{v}_2$), the components of the pseudo-command v (v_1 and v_2), the components of the pseudo-command v_{pd} (v_{pd1} and v_{pd2}), the components of the pseudo-command v_a (v_{a1} and v_{a2}), the components of the pseudo-command $\bar{v}$ ($\bar{v}_1$ and $\bar{v}_2$), and the components of the pseudo-command $\hat{v}_a$ ($\hat{v}_{a1}$ and $\hat{v}_{a2}$).

The convergence errors in figs. 8 and 9 are very good if the Federal Aviation Administration (FAA) accuracy requirements for Category III (the best category) [30] are analyzed; according to FAA Category III accuracy requirements, the lateral deviation (Y) must be less than 4.1 m; if the lateral error is between 4.1 m and 4.6 m, the aircraft meets the Category II precision standards, while if the lateral error is between 4.6 m and 9.1 m, the aircraft meets Category I precision standards. In our case, the stationary error is very close to zero after 30 seconds; this transient regime is good taking into account that the canceling process of aircraft lateral deviation with respect to the runway takes place long before the start of the two landing main stages in longitudinal plane (the glide slope phase and the flare phase). The reason that the design in this paper meets the requirement and achieves the design goal is that the neural networks have been used.

All the characteristics prove the new architecture's stability and its small overshoots; on the other hand, the differences between the two cases (with and without PCH block) are visible. The usage of a PCH block (when the actuator is nonlinear) does not modify the final values of the variables, but it decrease the transient regime period. For the same aircraft type, same direction controller, and radio-navigation system but with a proportional-derivative type control after the roll angle and a proportional type control after $\Delta\psi$ [6], there have been obtained performance inferior to those obtained with the new adaptive system for aircraft landing in lateral-directional plane (fig. 4), both from the transient regime and the overshoots' point of view; also, the results in this paper has been compared to the ones obtained in [28] where the authors have designed two new ALSs by using the H_∞ control, dynamic inversion, optimal observers, and reference models. The time regime period is better in [28] (almost 15 seconds) but the lateral deviation's overshoot is much larger (between 6.15 and 6.32 m for the first designed ALS (depending on the cross wind's velocity) and between 1.10 and 1.31 m for the second designed ALS); therefore, we can conclude that the neural networks-based adaptive controllers are more efficient than the conventional ones for aircraft landing in lateral-directional plane and, by using PCH blocks, the non-linear constraints are better handled.

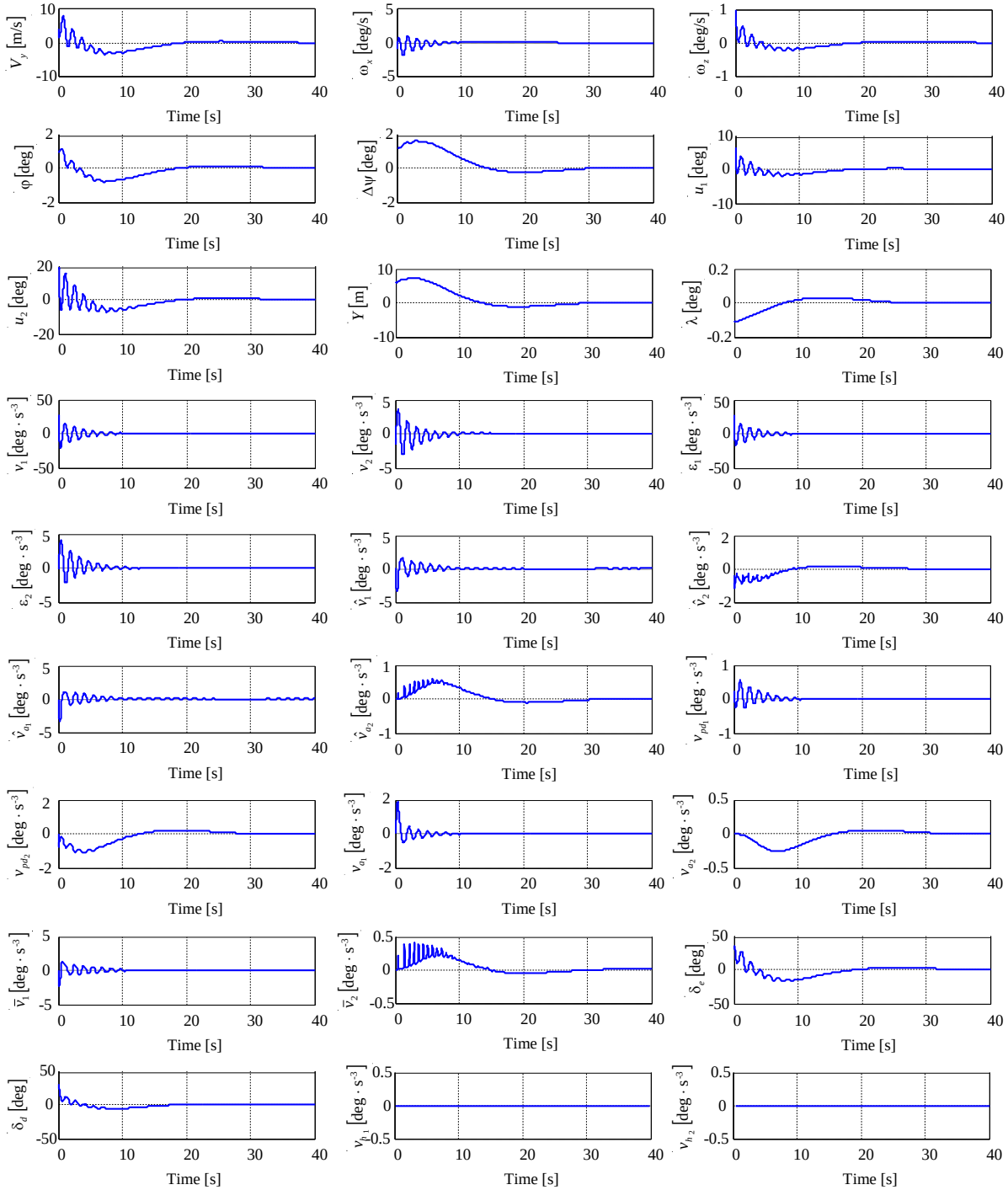

Fig. 8 Dynamic characteristics for aircraft motion in lateral-directional plane during landing (case 1: linear actuators)

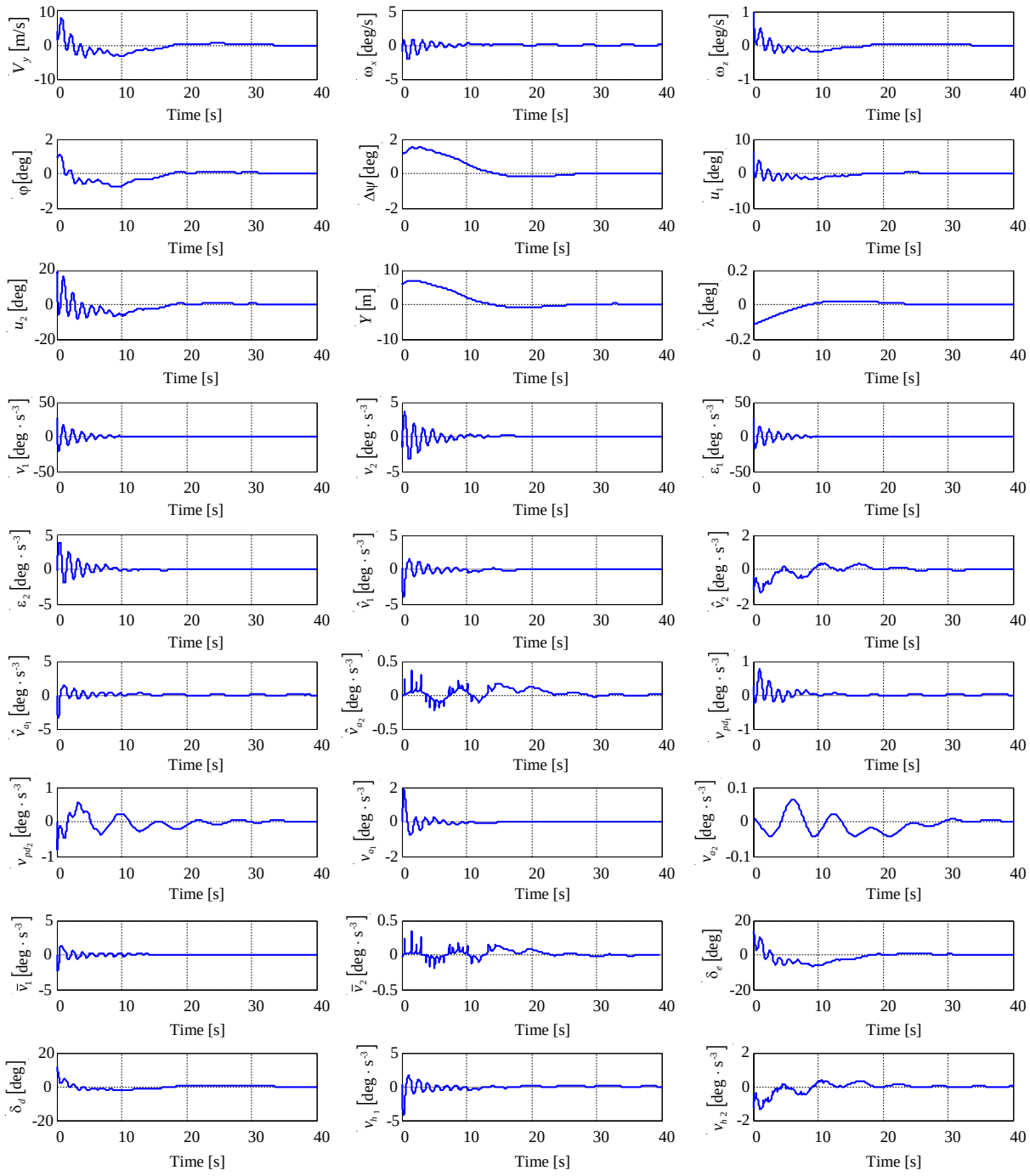

Fig. 9 Dynamic characteristics for aircraft motion in lateral-directional plane during landing (case 2: nonlinear actuators)

5. Conclusions

The automatic control system for aircraft guidance during landing (lateral-directional plane), consisting of an ILS and DME subsystems, is designed in this paper such that the angular deviation of aircraft with respect to the runway direction and the deviation of the flight direction relative to the runway are canceled. Also, the automatic control system cancels in steady regime the aircraft lateral deviation, its lateral velocity, the roll and the yaw angles, as well as their corresponding angular rates; the control of aircraft lateral-directional motion is achieved by modifying the calculated roll angle and the aircraft deviation with respect to the runway direction. The adaptive control system uses the dynamic inversion concept, a dynamic compensator, a neural network trained by the system's estimated error vector (signal provided by a linear observer), and a Pseudo Control Hedging block. We designed and software implemented all the components of the new landing system and we obtained the time histories of the main variables; the obtained characteristics prove the new architecture's stability and its small overshoots; there have been obtained better results than the ones in [6], especially due to the usage of neural networks-based adaptive controller and PCH block.

References

[1] Aron, I., Lungu, R., Cismaru, C., Sisteme de navigatie aerospatiala. Scrisul Romanesc Publisher, Craiova, 1989.

[2] McLean, D., Automatic Flight Control Systems. Prentice Hall Publisher, 1990.

[3] Lungu, M., Sisteme de conducere a zborului (Flight control systems). Sitech Publisher, Craiova, 2008.

[4] Lungu, R., Lungu, M., Grigorie, T. L., ALSs with conventional and fuzzy controllers considering wind shears and gyro errors. Journal of Aerospace Engineering, vol. 26, no. 4, 2012, pp. 794-813.

[5] Lungu, M., Lungu, R., Grigorie, L., Automat Control of the Aircraft Lateral Movement using the Dynamic Inversion. World Academy of Science, engineering and Technology, Paris, France, July 27-29, 2011, pp. 381-387.

[6] Lungu, M., Lungu, R., Grigorie, L., Automatic Command Systems for the Flight Direction Control during the Landing Process. Proceedings of International Symposium on Logistics and Industrial Informatics, August 25-27, 2011, Budapest, pp. 117-122.

[7] Che, J., Chen, D., Automatic Landing Control using H-inf control and Stable Inversion. Proceedings of the 40th Conference on Decision and Control, Orlando, Florida, USA, 2001, pag. 241-246.

[8] Lungu, R., Lungu M., Controlul automat al aeronavelor la aterizare (Aircraft automatic control during landing). Sitech Publisher, Craiova, 2015.

[9] Johnson, E.N., Calise, A.J., Pseudo-Control Hedging: A New Method for Adaptive Control. Navigation Guidance and Control Technology Workshop, November, 1-2, 2000.

[10] Vo, H., Sridhar, S., Robust Control of F-16 Lateral Dynamics. Int. Journal of Aerospace and Mechanical Engineering, 2008. pp. 80-85.

[11] Mori, R., Suzuki, S., Neural Network Modeling of Lateral Pilot Landing Control. Journal of Aircraft, no. 46, 2009, pp. 1721-1726.

[12] Calise, A., Johnson, E.N., Johnson, M.D., Corban, J.E., Applications of Adaptive Neural – Networks Control to Unmanned Aerial Vehicles. Journal of Harbin Institute of Technology, vol. 38, no. 11, 2006, pp. 1865-1869.

[13] Calise, A., Lee, S., Sharma, M., Direct Adaptive Reconfigurable Control of a Tailless Fighter Aircraft. Rev. American Institute of Aeronautics and Astronautics, Georgia, USA.

[14] Lungu, R., Lungu, M., and Grigorie, T. L., Automatic Control of Aircraft in Longitudinal Plane during Landing. IEEE Transaction on Aerospace and Electronic Systems, vol. 49, no. 2, 2013, pp. 1338-1350.

[15] Calise, A., Lee, H., Kim, N., High Bandwith Adaptive Flight Control. AIAA Guidance, Navigation and Control Conf. August 14-17, 2000.

[16] Johnson, E.N., Calise, A.J., Rysdyk, R., Shirbiny, E.A., Feedback Linearization with Neural Network Augmentation Applied to X-33 Attitude Control. AIAA Guidance, Navigation and Control Conference and Exhibit, August 14-17, 2000.

[17] Singh, S., Padhi, R., Automatic Path Planning and Control Design for Autonomous Landing of UAVs using Dynamic Inversion, American Control Conference Riverfront, St. Louis, MO, USA , 2009, pp. 2409-2414.

[18] Wagner, T., Valasek, J., Digital Autoland Control Laws Using Quantitative Feedback Theory and Direct Digital Design, Journal of Guidance, Control, and Dynamics, vol. 30, no. 5, 2007, pp. 1399-1413.

[19] Jang, J.O., Jeon, G.J., A parallel neuro-controller for DC motors containing nonlinear friction, Neurocomputing, vol. 30, 2000, pp. 233-248.

[20] Seshagiri, S., Khalil, H.K., Output feedback control of nonlinear systems using RBF neural network, IEEE Trans. Neural Networks, vol. 11, 2000, pp. 69-79.

[21] Wai, R.J., Development of New Training Algorithms for Neuro-Wavelet Systems on the Robust Control of Induction Servo Motor Drive, IEEE Transactions on Industrial Electronics, vol. 49, no. 6, 2002, pp. 1323-1341.

[22] Juang, J.G., Cheng, K.C., Application of neural networks to disturbances encountered landing control," IEEE Trans. Intell. Transp. Syst., vol. 7, no. 4, 2006, pp. 582-588.

[23] Saini, G., Balakrishnan, S.N., Adaptive Critic Based Neuro-Controller for Autolanding of Aircraft, Proceedings of the American Control Conference, Albuquerque, New Mexico, June 1997.

[24] Juang, J.G., Chang, H.H, Cheng, K.C., Intelligent Landing Control Using Linearized Inverse Aircraft Model, American Control Conference, vol. 4, 2001, pp. 3269-3274.

[25] Kee, P.E., Dong, L., Fuzzy-Logic Based Auto land Controller, Unmanned system Programme, Unmanned System centre, DSO National laboratories.

[26] Kumar, V., Rana, K.P., Gupt, V., Real-Time Performance Evaluation of a Fuzzy PI + Fuzzy PD Controller for Liquid-Level Process, International Journal of Intelligent Control and Systems, vol. 13, no. 2, 2008, pp. 89-96.

[27] Lau, K., Lopez, R., Onate, E., Neural Networks for Optimal Control of Aircraft Landing Systems, Proceedings of the World Congress on Engineering, vol. II, 2007, pp. 904-911.

[28] Lungu, R., Lungu, M., Automatic Control of Aircraft in Lateral-Directional Plane During Landing. Asian Journal of Control, 2015, DOI: 10.1002/asjc.1133.

[29] Tong, S.C., Li, Y.M., Feng, G., Li, T.S., Observer-Based Adaptive Fuzzy Backstepping Dynamic Surface Control for a Class of MIMO Nonlinear Systems. IEEE Transactions on Systems, Man, and Cybernetics, Part B: Cybernetics, vol. 41, no. 4, 2011, pp. 1124 - 1135.

[30] Braff, R., Powell, j.D., Dorfler, J., Applications of GPS to air traffic control, Global Positioning System: Theory and Applications, 1996; II: 327-374.